Saikiran Gopalakrishnan

School of Aeronautics and Astronautics, Purdue University, 701 West Stadium Avenue, West Lafayette, IN 47907 e-mail: gopalaks@purdue.edu

Nathan W. Hartman

Department of Computer Graphics Technology, Purdue University, 401 North Grant Street, West Lafayette, IN 47907 e-mail: nhartman@purdue.edu

Michael D. Sangid¹

School of Aeronautics and Astronautics, Purdue University, 701 West Stadium Avenue, West Lafayette, IN 47907 e-mail: msangid@purdue.edu

Integrating Materials Model-Based Definitions into Design, Manufacturing, and Sustainment: A Digital Twin Demonstration of Incorporating Residual Stresses in the Lifecycle Analysis of a Turbine Disk

Model-based definitions (MBDs) aim to capture both geometric and non-geometric data in digital product definitions using 3D computer-aided design (CAD) models, as a form of product definition baseline, to disseminate product information across different stages of the lifecycle. MBDs can potentially eliminate error-prone information exchange associated with traditional paper-based drawings and improve the fidelity of component details, captured using 3D CAD models. A component's behavior during its lifecycle stages influences its downstream performance, and if included within the MBD of a part, could be used to forecast performance upfront during the design and explore newer designs to enhance performance. However, current CAD capabilities limit associating behavioral information with the component's shape definition. This paper presents a CAD-based tool to store and retrieve metadata using point objects within a CAD model, creating linkages to spatial locations within the component. The tool is illustrated for storage and retrieval of bulk residual stresses developed during the manufacturing of a turbine disk acquired from process modeling and characterization. Further, variations in residual stress distribution owing to process model uncertainties have been captured as separate instances of the disk's CAD models to represent part-to-part variability as an analogy to track individual serialized components for digital twins. The propagation of varying residual stresses from these CAD models within the damage tolerance analysis performed at critical locations in the disk has been demonstrated. The combination of geometric and non-geometric data inside the MBD, via storage of spatial and feature varying information, presents opportunities to create digital twin(s) of actual component(s). [DOI: 10.1115/1.4048426]

Keywords: computer-aided design, computer-aided engineering, information management, knowledge engineering, model-based system engineering, process-modeling for engineering applications, virtual prototyping

1 Introduction

Traditional component design practice has largely been based on the geometry of the product being developed. Two-dimensional, paper-based drawings have been used to represent the geometric shape of an object (with different views as shown in Fig. 1(a)) with associated component design details for centuries. These drawings have been used to exchange the design definitions through different stages in the product lifecycle, such as manufacturing, quality inspection, and maintenance [2]. Typically, components are manufactured as specified by the geometric shape in the design, followed by physical testing to qualify the components, in order to meet the desired minimum performance per the design intent. This process of physically producing and then qualifying components is associated with multiple manufacturing trials that incur high costs and increased development time [3]. Based on the underlying physical structure and material composition, components respond differently

to their encountered environments, such as experienced thermomechanical deformation during the manufacturing process or applied loads during service. The evolution of the material structure during the processing route developed during the lifecycle, defined as the behavior [4] of the component, plays a crucial role in determining its final performance capabilities. Inclusion of behavioral information with the geometric shape in the design definition has an opportunity to aid in forecasting the component's performance upfront in the design process, thereby reducing expensive manufacturing trials and also enabling the exploration of a larger parameter space for new designs to meet the performance requirements, due in part to its inclusion in the digital artifact rather than in a separate location.

With the advancement in digital technology, predictive models of the manufacturing process have been evolving to simulate functional stages of the product lifecycle to determine the component behavior. In parallel, the design function has shifted from paper-based, 2D drawings to using 3D computer-aided design (CAD) models to represent and communicate design definitions [5,6]. Utilizing predictive models to simulate behavior and capturing these definitions in 3D CAD models provides an opportunity to include

¹Corresponding author.

Manuscript received March 20, 2020; final manuscript received August 24, 2020; published online October 16, 2020. Assoc. Editor: John Michopoulos.

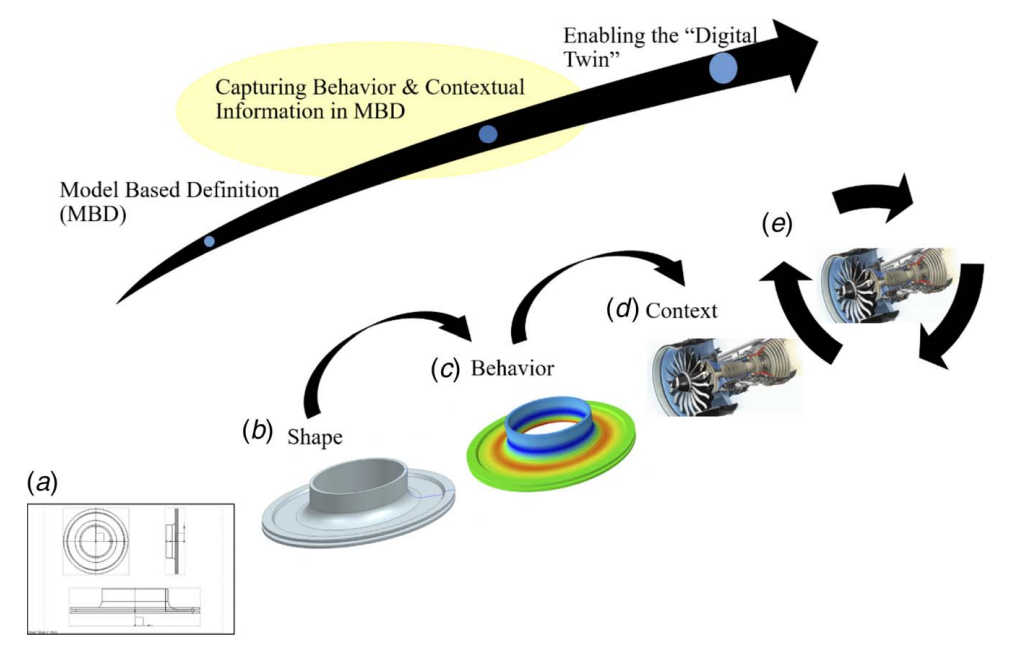


Fig. 1 The overarching vision to transition toward a digital twin by capturing the behavior definition within the design context. The figure represents this transition in design definition from (a) 2D paper drawing based to (b) CAD based to (c) MBD-CAD based to (d) Virtual Environment based [1] to (e) Lifecycle based [1].

behavioral information in the earlier stages of design, and to locate it securely in one location versus multiple disparate locations. However, current CAD models (shown in Fig. 1(b)) are limited to capturing the shape and geometric definitions (explicit definitions) and have very limited capability to include implicit definitions, such as the behavior developed as a result of the component's structure. In order to utilize the behavioral information to forecast the component's performance, CAD models need a mechanism to store and exchange these definitions, so as to function as a medium of exchanging design details, and the ability to recall the material performance definition in a useful form when needed in the future.

The use of 3D CAD models to include detailed product definitions, and replace 2D paper-based technical drawings, is also a goal of the concept of model-based definition (MBD). The aim is to use MBD-CAD models to communicate product definitions, in order to improve the quality of the exchanged product information and eliminate errors originating due to manual human intervention and interpretation of product metadata; both of which can lead to significant cost savings and acceleration of the design process cycle [2,5,7]. With this motive, CAD models have been used as an input to manufacturing processes, communicating the desired component geometry and the tolerances applied to its features [8]. However, the purpose of using the model-based approach has been expanding, beyond communication, for supplying the driving inputs within the downstream manufacturing stages and spanning across the entire product lifecycle [9–12]. With inclusion of the behavioral information within CAD models (Fig. 1(c)), the level and type of information captured and exchanged using MBD techniques exceed those of a simple geometric model.

Further, the MBD can be expanded to include contextual information, such as the operating environment details or the process environment details, that induces the behavior, as shown in Fig. 1(d). The contextual information from the MBD can provide details to simulations creating a virtual product environment to accurately replicate the behavior developed within the component and the performance of the component during its use. In other approaches to MBD, inclusion of behavior definition in the MBD from different stages of the product lifecycle could mean that the MBD would not be a single model, but would be a collection of

models with behaviors that originate from the different lifecycle stages. Such an integrated network of models, wherein the simulated behavior definitions can be exchanged across the product lifecycle, starts becoming the digital prototype of the designed component or the as-designed digital twin, as shown in Fig. 1(e). These as-designed twins, also known as product twin, can be used to simulate the component to forecast the performance capability during the design stage and prior to the production. The product twin can enable designs, which are inclusive of behavior definitions, to meet desired performance requirements [13,14]. In order to progress toward this vision, the current work focuses on closing the gap of including behavior definitions within CAD models and enabling their exchange, while integrating definitions between the models.

The concept of MBD can be applied to include manufacturing process-induced residual stresses within design definitions of a component, as they influence the component production process and performance such as durability and damage tolerance [15]. Residual stresses influence the fabrication of a component, especially in a multi-stage manufacturing process. Components encounter thermomechanical loads during processes such as forging or heat treatment, which induces permanent localized strain gradients. These strain gradients manifest as residual stress distributions within the component [16]. These stresses are classified as bulk residual stresses or Type I, when they equilibrate over the length scale of the component dimensions. The residual stresses redistribute after each stage during the manufacturing process and influence the succeeding manufacturing steps [17]. Due to excessive residual stresses, components can distort during the machining stages, exceeding the geometric tolerances of specific features [18,19]. Incorporating residual stress distributions from process modeling steps within the design definition can provide the residual stress distribution knowledge and enable optimizing the process parameters to avoid part distortion and scrap for a fixed design of the component. Process modeling tools, such as DEFORM [20], simulate the manufacturing process steps to predict these bulk residual stress distributions from each manufacturing step.

Post manufacturing, the residual stress distribution developed within the component, influences its performance, especially the fatigue life of the component [21,22]. For a crack or a flaw at a location within the component, compressive residual stress fields inhibit

crack growth and delays fatigue failure, whereas tensile residual stress fields accelerate crack growth and debit the fatigue life. However, residual stresses are not typically included in lifetime analyses, but by taking residual stresses into account during the lifing process, more informed decisions can be made about the inspection and maintenance schedules and can even result in life extensions of the components. For instance, John et al. [23] have observed an approximate twofold increase in lifetime based on a damage-tolerant analysis by including the 30% retained compressive residual stress from shot peening. McClung et al. have demonstrated the integration of residual stress fields from DEFORM process model with probabilistic damage-tolerant analyses, specifically DARWIN (Design Assessment of Reliability with INspection), for life prediction analysis at critical zone locations [24]. Including residual stress fields from models within design definition, and using them in structural analysis and lifting models, requires a method to store and exchange the spatially varying residual stresses in a form that will persist when used within multiple software tools across the lifecycle.

In order to effectively utilize residual stresses in the design process and consume this information in the lifecycle analysis, the associated uncertainties in quantifying the residual stresses must be also be captured, as they influence the uncertainties in the downstream life predictions. Process modeling simulations have uncertainties in the predicted residual stresses originating from the uncertainties in the process model input parameters [25]. Residual stresses, determined from characterization techniques [26], have been used to validate process models. A recent study [27], as a part of Metals Affordability Initiative Foundational Engineering Program (MAI-FEP), illustrated validation of bulk residual stress from process modeling predictions in a Nickel-based superalloy turbine disk using measurements from characterization techniques. Using the validated process model, the overall goal of the study was to optimize the disk geometry and processing parameters, in order to obtain favorable residual stresses to meet performance requirements. This would require capturing the variations in predicted residual stresses from process models within the design definition and propagating the uncertainties to structural analysis and lifing models.

With the overarching aim to develop a capability to include behavioral information from product lifecycle stages within the design definition, and store it in a form to allow propagation of this information for downstream performance analysis, the current work presents a CAD-based tool to store and exchange metadata. The mechanism used by the developed tool and its software framework has been detailed in Sec. 2. This tool has been illustrated with a use case to store the manufacturing-induced bulk residual stresses in a Nickel-based superalloy turbine disk component, obtained from (a) process modeling and (b) experimental characterization, from datasets obtained via the MAI-FEP study (Sec. 3) [27]. Further, residual stress distributions representing three cases of variations from the nominal values, due to process model uncertainties or analogous to part-to-part variations, have been generated and stored in three instances of the disk's CAD models. The stored residual stress fields with their associated variability have been exchanged using the CAD models by utilizing the developed tool and incorporated within damage-tolerant analyses (Sec. 4). Finally, the conclusions are provided in Sec. 5.

2 Method and Implementation

In order to include behavioral information within a design model, a CAD-based tool has been developed to store and retrieve metadata using the CAD model. The detailed description of the tool and its development has been presented in Ref. [28]. The functionality provided by the tool is to import externally stored metadata into the CAD software's environment, in order to store and retrieve the associated metadata, such as behavior attributes, at spatial locations within the model. To provide background and implementation

details of the tool for the current study, the methodology and software framework are described in this section.

2.1 Embedding Methodology. In order to associate metadata with component feature locations, the tool has been developed to create spatial points within the CAD model to store the metadata. Points have been used to store data as they are fundamental geometric objects that can be used to create other geometric entities such as lines, arcs, surfaces, and solids. This enables storing the metadata with precision on fine topological features such as a vertex, on the component edges, and surfaces or even within the bulk volume. Within the CAD environment, each point object is defined by its location coordinates (x,y,z). The tool has been developed to store metadata as name value pairs attached to these point objects, which defines the attribute name and the value of the attribute. Once stored, the location of each of the points within the geometric space of the model acts as a spatial index for the associated metadata. These point objects with the stored metadata values are henceforth referred to as attribute markers in this paper. An attribute marker can store multiple metadata attributes. For instance, multiple behavior definitions that apply to a particular location can be associated using a single point. This can be applied for storing the components of tensorial quantity, such as residual stresses. The data types that can be stored currently using the tool are numbers and textual information. Attribute markers follow a schema which is as follows: [(x position), (y position), (z position), (Name of Attribute 1), (Value of Attribute 1), (Name of Attribute 2), (Value of Attribute 2) ... (Name of Attribute n), (Value of Attribute n)]. The attribute names are user defined and can comprise alphanumeric data with spaces, whereas the attribute values must be a numeric value of floating-point data type. The tool has been developed to allow importing and storing datasets, which are structured by nature, and by following this schema, they enable querying and searching for data retrieval.

2.2 Software Framework. The embedding tool has been developed as a plug-in for the CAD tool, executed by the user while launching the CAD software (Fig. 2(a)). The integration of the embedding tool with the CAD software has been performed using the CAD tool's Software Development Kit (SDK), which allows making use of the command-structure functions specific to the CAD tool. The only CAD-dependent functionalities used for integration are the loading and unloading process of the plug-in, while opening and closing the CAD software, respectively. Thus, the embedding plug-in can be easily switched and used with a different CAD tool by using the CAD tool's specific SDK's functionalities. The current implementation of the tool is shown for Siemens NX 10.0 CAD tool. Once the tool is loaded within the CAD software, the user can interact with the model to include external datasets by storing and retrieving the stored metadata directly from the CAD model.

The workflow for the metadata storage process using the tool is represented by the flow diagram shown in Fig. 2(b). The process is initiated by the selection for a data storage option. The tool allows two methods of importing metadata. For small sets of data, attribute markers can be created manually by clicking the location where the markers apply within the CAD model. On the other hand, larger sets of metadata can be imported using the bulk data import option. The bulk import method creates a collection of attribute marker points or a point cloud, each with its associated metadata set. In order to utilize this method of storage, the imported data must be structured following the attribute marker schema (described in Sec. 2.1) in a comma space value (CSV) file. While creating the CSV file and defining the spatial coordinates of the attribute markers, if there are differences in the coordinate systems between the CAD model and the external software/data sources where the attribute marker datasets originate, a suitable correction using translations and/or rotations must be applied manually to ensure consistent storage of the spatial metadata within the

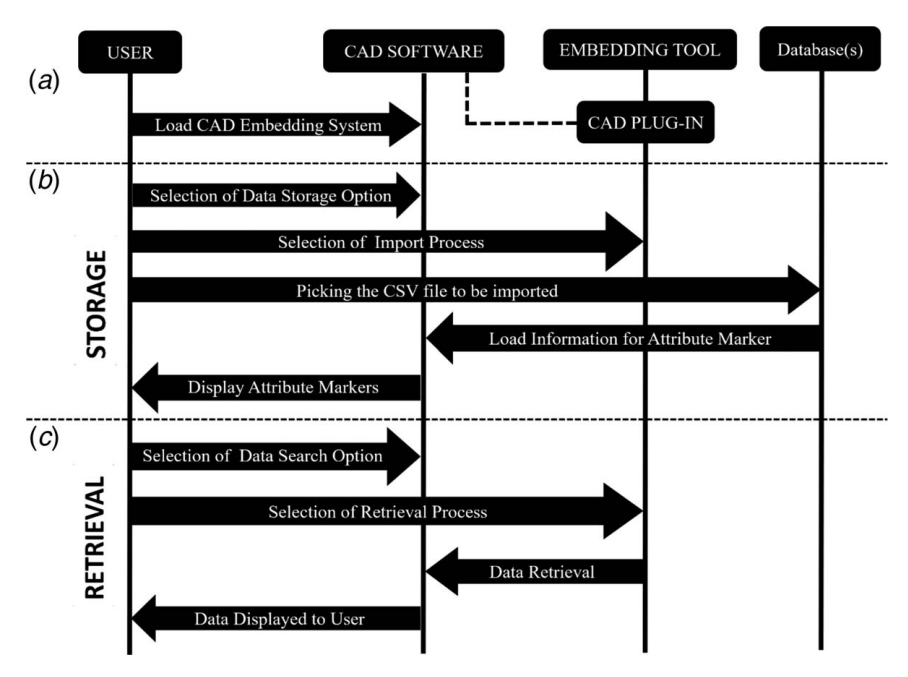


Fig. 2 A flowchart describing the CAD-based embedding tool's software architecture, including the (a) integration of the tool with the CAD software, (b) data storage process, and (c) data retrieval process

component's CAD model. During the import process, the CSV file is imported from the database and the tool generates attribute markers from the available datasets. In the current study, behavior definition across the entire component geometry has been captured using the bulk import mechanism.

The search and retrieval of stored metadata can be initiated using the attribute marker entities via one of the following options: either the attribute name or the attribute marker location. The metadata retrieval workflow has been presented in Fig. 2(c). To search based on attribute names, the embedding tool filters and extracts all the spatial locations which have the particular attribute defined, and to extract attribute values from a specific location within the model, the tool executes a PYTHON script that searches for an attribute marker using its location coordinates within the CAD model, with the attribute markers being displayed using the CAD tool. For locations within the model where there is no stored metadata, the current implementation extracts and returns the nearest attribute marker. The extraction capability of the tool enables communicating the location-specific behavioral metadata directly using the CAD model, which provides a significant

advantage since many embedded attribute values are typically lost or corrupted during data translation using neutral data formats.

3 Residual Stress Use Case

In order to illustrate how the developed tool enhances a CAD model to store behavioral information and starts forming a model-based definition, a use case has been implemented in the current work for bulk residual stresses generated during the manufacturing process of a turbine disk. The goal is to associate residual stress fields to locations within the component's CAD model and exchange the stored residual stresses for damage tolerance analyses, directly using the CAD model. For implementing the use case, various tools/software(s), data sources, and codes have been utilized along with the embedding tool. The flow of data between them is shown in Fig. 3. Residual stress data have been acquired from both experimental characterization, as well as from a process modeling tool (DEFORM), both of which are stored within the CAD model using the embedding tool. Additionally, in order to

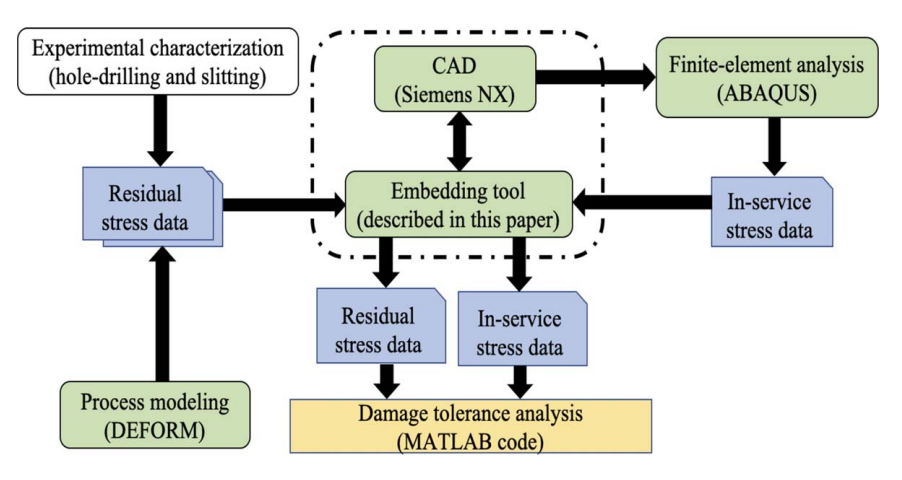


Fig. 3 A schematic representing the flow of data between various tools/software(s), codes, and other data sources for implementing the use case

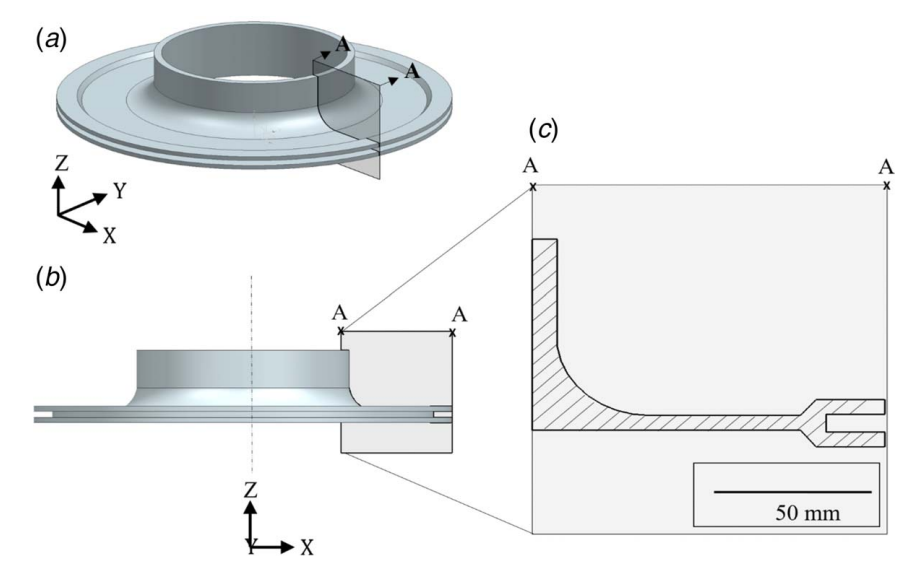


Fig. 4 Views of the turbine disk model, namely, the (a) trimetric view, (b) front view, and (c) 2D axisymmetric view. The section view A-A shows the 2D axisymmetric view of the turbine disk.

produce in-service stresses in the component for damage tolerance analysis, a finite element (FE) analysis tool has been used to simulate the structural characteristics of the component. Herein, the CAD model provides the component geometry for the analysis and the resulting in-service stress fields are further stored within the CAD model using the embedding tool. Finally, both the stored residual stresses and in-service stresses are retrieved from the CAD models via the embedding tool and utilized within a damage tolerance analysis code. With the overarching aim of implementing the use case, the following section describes the component model creation, residual stress data acquisition techniques, and data preparation for storing using the tool.

3.1 Turbine Disk Computer-Aided Design Model. The first step was to create a design model using the CAD tool, representing the geometric definition of the turbine disk. Figure 4(a) represents the trimetric view of the turbine disk component model. A disk is an axisymmetric component (in Fig. 4(c)), which is to say the geometry is symmetric about the *z*-axis passing through the centroid of the disk and shown as a 3D model in Fig. 4(b). This CAD model represents the as-designed nominal disk geometry.

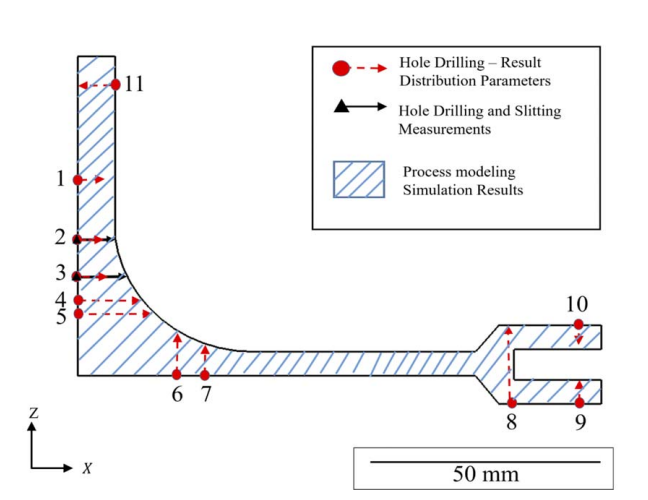


Fig. 5 Locations in the CAD model of the turbine disk, where residual data are being stored, as represented on the 2D axisymmetric view of the disk

3.2 Residual Stress Data Acquisition and Import Dataset Preparation. The residual stress data has been acquired using experimental characterization techniques within the MAI-FEP program [27], namely, hole-drilling and slitting, performed at feature locations 1–11 and 2–3, respectively (as defined in Fig. 5), within the disk. Process modeling, using DEFORM, has been used to determine the full-field residual stresses across the entire component. Further, cases of variations in the residual stress distribution, arising due to uncertainties in the process modeling [25], have also been generated. These residual stress datasets have been structured following the attribute marker schema and stored at locations (as displayed in Fig. 5) within the CAD model of the disk.

3.2.1 Residual Stress Data Acquisition: Experimental Characterization

3.2.1.1 Hole-drilling. The first characterization method that has been used to acquire residual stress data is hole-drilling. Hole-drilling is a mechanical characterization technique used to determine the near-surface residual stresses as a function of depth. The technique involves drilling of a hole in steps from the component

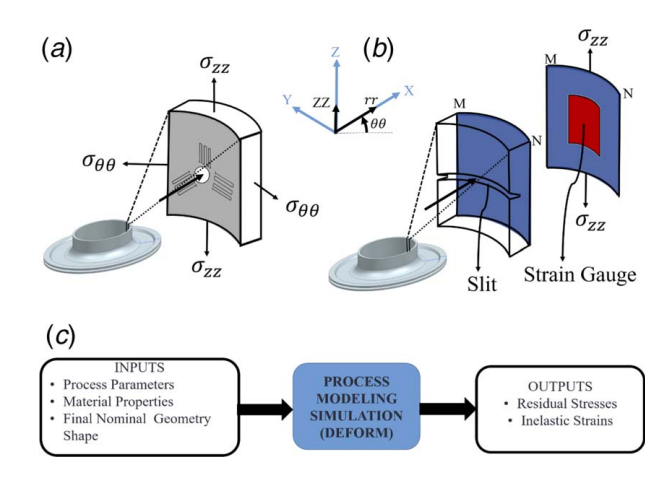


Fig. 6 Residual stress data acquisition techniques: (a) schematic of the hole-drilling experiment, (b) schematic of slitting experiment, and (c) flow diagram representing the DEFORM process modeling

surface along the thickness direction, which leads to relaxation of the residual stresses and deforming of the component accumulated during initial manufacturing. A strain gage rosette is placed on the surface, to measure the associated deformation at each step. The schematic of the hole-drilling setup is shown in Fig. 6(a). The measured deformation is used to back calculate the in-plane residual stress components, originally present, at the hole location from the surface.

Hole-drilling measurements have been performed on a physical turbine disk component at locations 1–11, as shown in Fig. 5, at positions around the disk's axis at 15 deg, 105 deg, 195 deg, and 285 deg to capture the variation in the measured residual stresses around the 3D component. In feature locations 1–5 and 11, distribution parameters of hoop $(\sigma_{\theta\theta})$, axial (σ_{zz}) , and shear $(\sigma_{\theta z})$ components of the residual stress have been obtained, whereas in locations 6-10, statistics of radial (σ_{rr}) , hoop $(\sigma_{\theta\theta})$, and shear $(\sigma_{r\theta})$ stress components have been obtained. This dataset has been organized, with distribution parameters for each stress component as a scalar entry, as follows: [x,y,z, Mean (Hoop Stress), Numeric value, Standard Deviation (Hoop Stress), Numeric value, Mean (Axial Stress), Numeric value, Standard Deviation (Axial Stress), Numeric value, Mean (Shear Stress), Numeric value, Standard Deviation (Shear Stress), Numeric value] at locations 1–5 and 11 and [x,y,z, Mean (Radial Stress), Numeric value, Standard Deviation (Radial Stress), Numeric value, Mean (Hoop Stress), Numeric value, Standard Deviation (Hoop Stress), Numeric value, Mean (Shear Stress), Numeric value, Standard Deviation (Shear Stress), Numeric value 1 at locations 6–10. Further, at locations 2 and 3 (Fig. 5), the measured axial residual stress component (σ_{zz}) is stored as a function of distance from the surface. Following the schema, the dataset has been created in a CSV file as follows: [x,y,z, Axial Stress (HOLE-DRILLING), Numeric Value], wherein y=0 and z=constant for each feature location with varying x position in the dataset.

3.2.1.2 Slitting. Slitting analyses has been used as the second technique to generate residual stress data for the turbine disk component. Similar to hole-drilling, slitting also uses a strain relaxation approach to measure the associated deformation. Unlike drilling of

holes, slitting involves cutting of slits from the surface, in steps along the thickness direction with a strain gage placed on the end surface orthogonal to the slit to measure the associated deformation (Fig. 6(b)). The measured deformation is used to back calculate the originally present axial residual stress (σ_{zz}) component as a function of slit depth. Slitting has been performed on the turbine disk, starting at locations 2 and 3, as shown in Fig. 5. Following the schema, the dataset has been created in a CSV file as follows: [x,y,z,Axial Stress (SLITTING), Numeric Value], wherein y = 0 and z = constant for each feature location with varying x position in the dataset.

3.2.2 Residual Stress Data Acquisition: Process Modeling. The manufacturing processing route of the turbine disk that includes forging, heat treat, and machining operations has been simulated to determine the induced residual stress distributions using DEFORM [20], as part of the MAI-FEP [27]. The inputs to the simulation include the initial billet geometry, process parameters, material properties, and the final nominal geometry shape (Fig. 6(c)). The analysis has been performed using axisymmetric quadrilateral elements. The mesh included 2756 elements with average mesh size of 0.7 mm. For each of these elements, four residual stress components, namely, the radial stress (σ_{rr}) , hoop stress $(\sigma_{\theta\theta})$, axial stress (σ_{zz}) , and shear stress (σ_{rz}) , are generated. The element centroids from the process model are used to create attribute markers, in which the four residual stress components are stored. Since there was no coordinate system mismatch between the CAD model and the process model, the coordinates of elemental centroids can be directly used to create the attribute markers. A MATLAB script has been written to create the import dataset for the embedding tool from the process modeling results file (DEFORM keyword file). Following the schema, the attribute markers dataset in a CSV file have been created as follows: [x,y,z, Radial Stress, Numeric Value, Hoop Stress, Numeric Value, Axial Stress, Numeric Value, Shear Stress, Numeric Value], wherein x,y,z are the elemental centroid positions.

3.2.3 Residual Stress Data Acquisition: Process Modeling Variations due to Model Uncertainty. In order to demonstrate

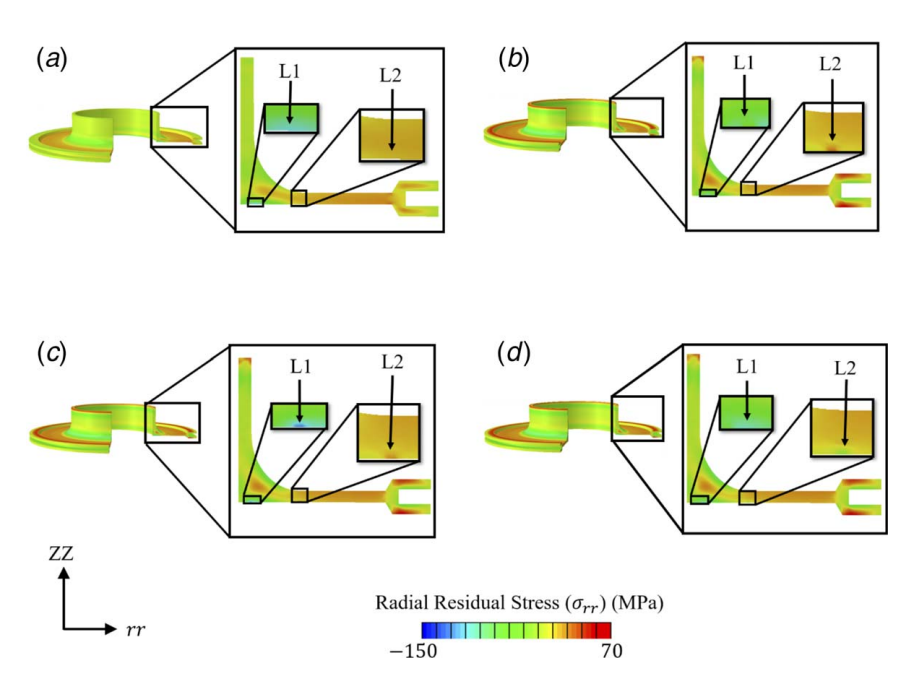


Fig. 7 Visualization of the predicted radial component (σ_{rr}) of residual stress datasets, with variations arising due to process modeling uncertainties highlighted at locations L1 and L2: (a) nominal residual stress distribution from DEFORM simulation defined as Turbine Disk Model 1; (b, c, d) three cases of varying residual stress distributions generated to represent process modeling variations termed as Turbine Disk Model 2, Turbine Disk Model 3, and Turbine Disk Model 4, respectively

potential part-to-part variations that can be forecasted in the as-designed digital twins or tracked among individual components of the as-built digital twins, variations in the residual stresses were studied based on the reported uncertainties of the available dataset [25]. Three cases of varying residual stress distributions have been created, in addition to the available nominal residual stress distribution for this study, to represent cases of part-to-part variations. To create these updated residual stress distributions, the nominal radial stress values were initialized as predefined stress fields with perturbations at locations L1 and L2 (as shown in Fig. 7(a)) within an ABAQUS finite element model, followed by a relaxation step to redistribute and equilibrate the stress fields to generate new residual stress distributions. All the surfaces of the 2D axisymmetric disk model were constrained from displacing in the normal direction, similar to a heat treatment process analysis. The choices of percentage changes for the perturbation were made, such that the change in the final radial residual stresses from the nominal values, after running the analysis step, were within the radial stress uncertainty bounds reported for a location between L1 and L2 in Ref. [25]. The updated final radial residual stress percentage changes for the three generated cases at location L1 were 87%, -20.35%, and 67.26% and at location L2 were 159%, 109.09%, and -172%. The contour plots of the original nominal radial residual stress distribution, and the three instances of distributions arising due to model uncertainty (analogous to part to part variation), are represented in Fig. 7(a) and Figs. 7(b)-7(d), respectively.

4 Results and Discussion

4.1 Inclusion of Residual Stress Fields Within CAD Model of Turbine Disk. The residual stress datasets, that have been acquired and re-organized (Sec. 3.2) as per the attribute marker schema (described in Sec. 2), have been imported and stored

within the CAD model of the turbine disk using the embedding tool. The four cases of residual stress fields, representing part-to-part variability, have been stored within four instances of CAD models, as shown in Fig. 8(a)(i-iv) based on the nominal turbine disk geometry, using the bulk data import method in the developed tool. The detailed representation of the enhanced CAD model of the disk with nominal residual stresses (Fig. 8(a)(i)) obtained from process modeling and characterization techniques is shown in Fig. 8(b). The attribute markers are represented as "+", which is the default representation of a point object in the CAD software used in this study. In the process of including the residual stresses, the preprocessing steps involved (a) preparation of the CSV import file with point object information and (b) importing the data to create point objects within the CAD model, both being computationally feasible and taking less than 2 min. After storing the residual stress datasets, the native CAD model's file size increased moderately, from 166 kB to 742 kB, while still remaining as a sufficiently small file size to promote data exchange.

Attribute markers have been created across the component volume to store residual stress fields from process modeling for all of the 2D axisymmetric components (radial stress (σ_{rr}), hoop stress $(\sigma_{\theta\theta})$, axial stress (σ_{77}) , shear stress (σ_{77}) of the stress tensor (shown in Fig. 8(c)), enabled by the capability of the framework to store multiple attributes at a single location. This capability has also been used to capture the variations in measured residual stress components from hole-drilling at feature locations 1-11, by creating attribute markers on the surface of the disk at these feature locations. The use of point objects allows storing of metadata with fine precision. For instance, the measured gradient of the axial stress component (σ_{zz}) near the surface at locations 2 and 3 have been captured by creating attribute markers at the holedrilling measurement locations. To store axial residual stress (σ_{77}) from slitting, 37 attribute markers have been created within 7.62 mm from the surface—one such marker shown in Fig. 8(d).

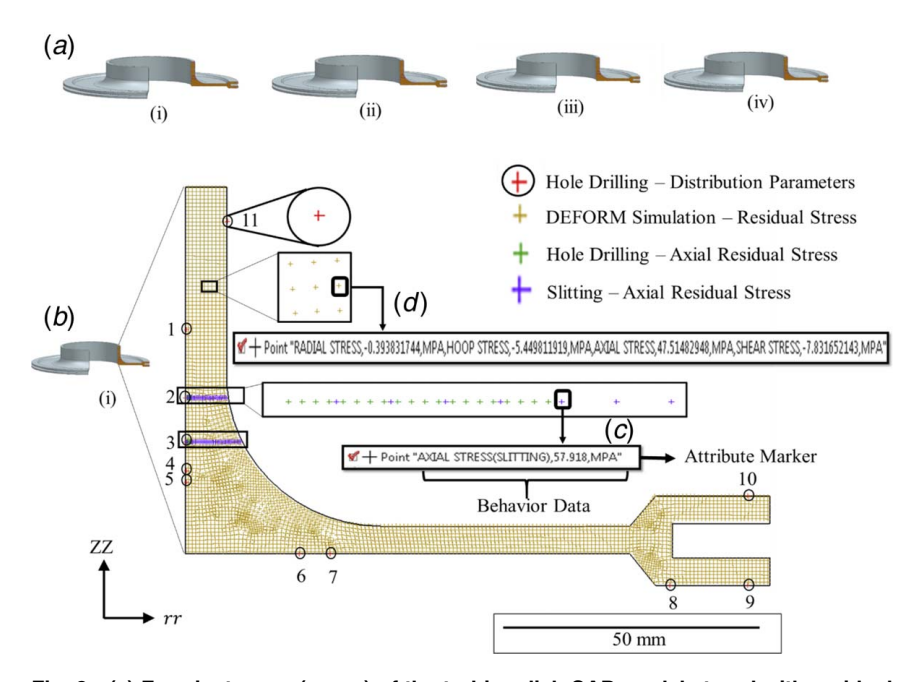


Fig. 8 (a) Four instances (cases) of the turbine disk CAD model stored with residual stress definitions from: (i) Turbine Disk CAD Model 1 (nominal residual stresses from the process modeling) and (ii), (iii), and (iv) Turbine Disk CAD Model 2–4, respectively with residual stress data to represent part-to-part variations; (b) 2D axisymmetric view of the 3D CAD model of the turbine disk with attribute markers storing the nominal residual stress data; (c) example of an attribute marker with residual stress data from process model, following the schema structure (attribute name followed by attribute value, in pairs, storing multiple attributes); and (d) example of an attribute marker with residual stress data from experimental characterization (Slitting), following the schema structure (attribute name followed by attribute value, at a measurement location)

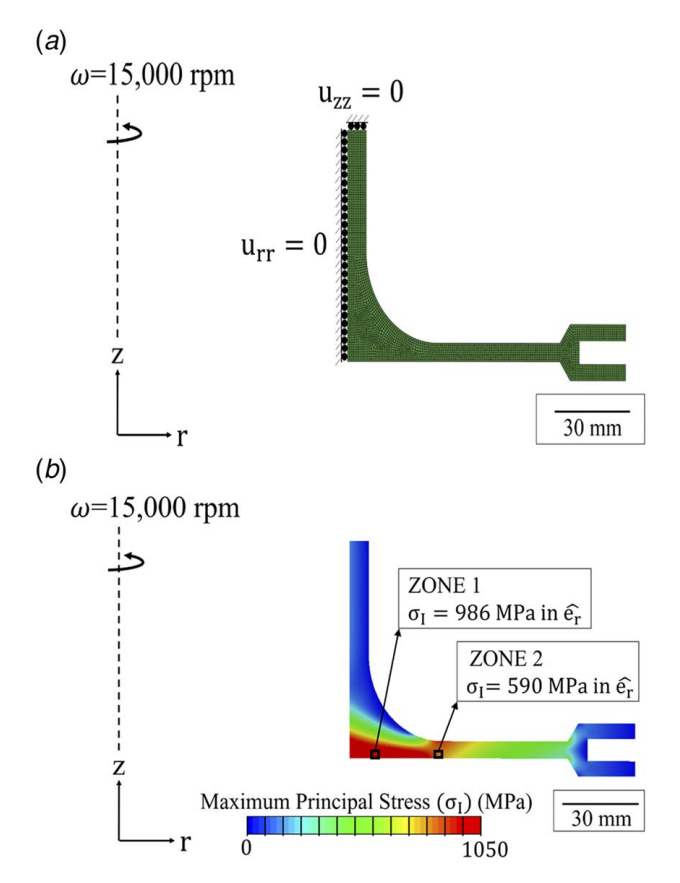
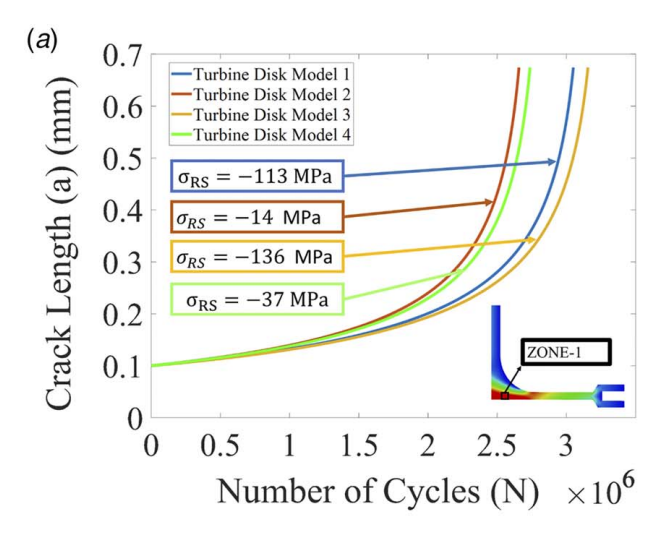


Fig. 9 Finite element model of the in-service disk: (a) 2D axisymmetric model geometry with quadrilateral mesh elements, centrifugal load, and boundary conditions and (b) maximum principal stress distribution generated in the disk, from in-service rotation, marked with two selected high-stress zones for damage-tolerant-based lifting analysis

To store the near-surface residual stresses from hole-drilling, 20 attribute markers have been created within a 0.9652 mm width from the surface. The demonstrated ability to store experimentally measured data, alongside the predicted model data, is necessary for the verification, validation, and uncertainty quantification procedures to build trust in the predictive models [29] and is needed to certify the usage of individual components whose design relies on modeling results. This demonstrated ability also becomes critically important for changing business models across product portfolios with increasingly long lifecycles, particularly as it relates to sourcing and provisioning maintenance and sustainment services.

4.2 Incorporation of Residual Stress Definitions in Fatigue Life Analysis. The stored residual stress fields can be retrieved from the CAD models using the presented tool and utilized, along with the stresses generated within the disk during its service, for damage-tolerant based fatigue life analysis. During service, turbine disks encounter varying rotation speeds and are subjected to fatigue loading. In order to obtain the in-service stresses generated in these disks, a FE simulation has been performed. The analysis has been performed for the maximum load case, while assuming the minimum applied load to be zero, i.e., when the disk is at rest (hence the fatigue stress ratio is R = 0). The model used for this analysis, with the loads, boundary conditions, and the mesh are as shown in Fig. 9(a). The inner bore region of the disk has been imposed with a displacement constraint in the radial direction $(u_{rr} = 0)$ and the upper surface has been constrained in the axial direction $(u_{zz} = 0)$ to simulate the constraints imparted by the shaft on the disk. For this simulation, the only load that



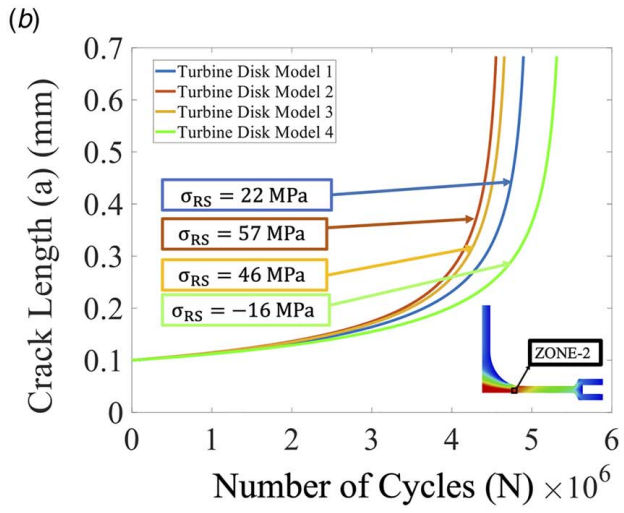


Fig. 10 Crack length versus number of cycles in the two critical locations: (a) zone 1 and (b) zone 2, including the resulting variability in performance based on the part-to-part variation of the residual stress fields

has been considered is the load applied due to spinning of the disk. A centrifugal load has been applied on the disk with a spin speed of $\omega = 15,000\,$ rpm [30]. The outer blade loads, and shrink fit loads due to attaching the disk to the shaft, have been ignored. Linear elastic, isotropic material properties of IN718, which are the Young's modulus $E = 170\,$ GPa and Poisson's ratio (ν) = 0.3 at 600 °C [30], as well as the density (ρ) = 8220 kg/m³, have been applied to the disk section. Linear quadrilateral elements have been used to mesh the model with element size of 0.7 mm and 2765 elements, similar to process modeling simulation (Sec. 3.2.2).

The maximum principal stress ($\sigma_{I,max}$) distribution within the disk, obtained from the FE analysis is as shown in Fig. 9(b). In order to store these in-service stresses within the turbine disk model, so as to extract and use them for life analysis, a new CAD instance of the disk was created. From the analysis model, the location coordinates of FE centroids have been computed using the nodal coordinates. The elemental centroid locations along with the maximum principal stresses at each of these elements form the attribute markers to be imported and stored within the new CAD model instance. In order to account for the difference in coordinate systems between the FE model and the CAD model (as discussed in Sec. 2.2), a manual correction has been applied to the position coordinates of the attribute markers using suitable rigid body translations, prior to importing the dataset. Finally, by using

the embedding tool, these attribute markers with $\sigma_{I,max}$ have been imported and stored at these locations within the disk.

In order to perform fatigue life prediction analysis based on damage-tolerant approach, two zones have been selected from the high-stress regions within the disk (shown in Fig. 9(b)). The maximum principal stresses in these zones are $\sigma_{I,max}$ = 986 MPa in zone 1 and $\sigma_{I,max}$ = 590 MPa in zone 2. In each of these zones, a blunt tip crack with the shape of a U notch of initial length a_i = 0.10 mm, that can be missed during crack inspection [31], has been assumed to be present. The analysis has been formulated such that the maximum principal tensile stresses will lead to opening of the crack, following mode I crack growth. Since the directions of $\sigma_{I,max}$ in these zones are along the radial direction (\widehat{e}_r) , the crack is assumed to be growing along the axial direction of the disk (\widehat{e}_z) , such that the tensile maximum principal stresses at these zone locations act as the crack opening stresses. The estimated life for this crack to grow to a critical final crack length a_f has been computed. The final length (a_f) for each zone has been determined as the length at which stress intensity factor (K_I) [32] reaches the fracture toughness (K_{IC}) $(K_{IC} = 85 \text{ MPa}\sqrt{m} \text{ [30]})$. To estimate the number of cycles (N_f) for the initial crack length (a_i) to grow into a final crack length (a_f) , a formulation incorporating both the residual stresses and the service stresses has been used [33].

The Paris law (Eq. (1)) provides the relationship during stage II crack growth, between the rate of crack propagation (da/dN) and effective stress intensity factor (ΔK_{eff}), which is the driving force for the crack growth. C, n are Paris constants for IN718, with values taken as $2.83 \times 10^{-17} \left(\frac{\text{mm}}{\text{cycle}}\right) / \text{MPa} \sqrt{\text{mm}}$ and 3.213, respectively, at $R \sim 0$ at elevated temperature [34]

$$\frac{da}{dN} = C(\Delta K_{eff})^n \tag{1}$$

The Walker model [35] modifies the effective stress intensity range (ΔK_{eff}) in the Paris law (Eq. (1)) as shown in Eq. (2), to account for the effects of changes in the R ratio on the crack growth rate. Using this formulation, the effect of residual stress has been incorporated in the stress ratio R (shown in Eq. (3)), by linear superposition of the maximum principal applied stresses

(i.e., $\sigma_{I,min}$ corresponding to the minimum applied load and $\sigma_{I,max}$ corresponding to maximum applied load) with the residual stress component (σ_{RS}) along the direction of the maximum principal applied stress. Equation (3) is valid for $R \ge 0$ and takes the value of 0 for cases when R < 0. In the present analysis, $\sigma_{I,min} = 0$ and $\sigma_{I,max}$ is obtained from the FE analysis. m is the material dependent Walker exponent (m = 0.5) [36]

$$\Delta K_{eff} = K_{max} (1 - R)^m \tag{2}$$

$$R = \frac{\sigma_{I,min} + \sigma_{RS}}{\sigma_{I,max} + \sigma_{RS}} \tag{3}$$

 K_{max} is the stress intensity factor corresponding to maximum load, which has also been superimposed with residual stress as shown in Eq. (4), wherein F(a/w) is the geometric correction factor, w is the width of the section and a is the crack length

$$K_{max} = (\sigma_{I,max} + \sigma_{RS})F\left(\frac{a}{w}\right)(\pi a)^{\frac{1}{2}}$$
 (4)

F(a/w) varies for the crack placed in each of the zones and is a function of a and w. The width of the two sections in the zones analyzed are $w_1 = 27.21$ mm and are $w_2 = 5.89$ mm, respectively. A FE approach was used to obtain the geometric correction factor for the turbine disk, for details please refer to Appendix. Using the critical stress intensity factor, K_{IC} , and appropriate geometric correction factor, the final crack length has been calculated for each of the zones as $a_{f,Zone1} = 0.6742$ mm and $a_{f,Zone2} = 0.6832$ mm.

By substituting Eqs. (2)–(4) in Eq. (1) and rearranging dN in terms of da, we can obtain the expression to compute the life in each zone for the crack to grow from the initial to final length by integrating between a_i to a_f (as shown in Eq. (5))

$$N_{f} = \frac{1}{(C(\sigma_{I,max} + \sigma_{RS})(1 - R)^{m})^{n}} \int_{a_{i}}^{a_{f}} \frac{da}{\left(F\left(\frac{a}{W}\right)(\pi a)^{\frac{1}{2}}\right)^{n}}$$
 (5)

For extracting $\sigma_{I,max}$ and σ_{RS} from the CAD models, the location-based retrieval method of the developed tool has been used. The

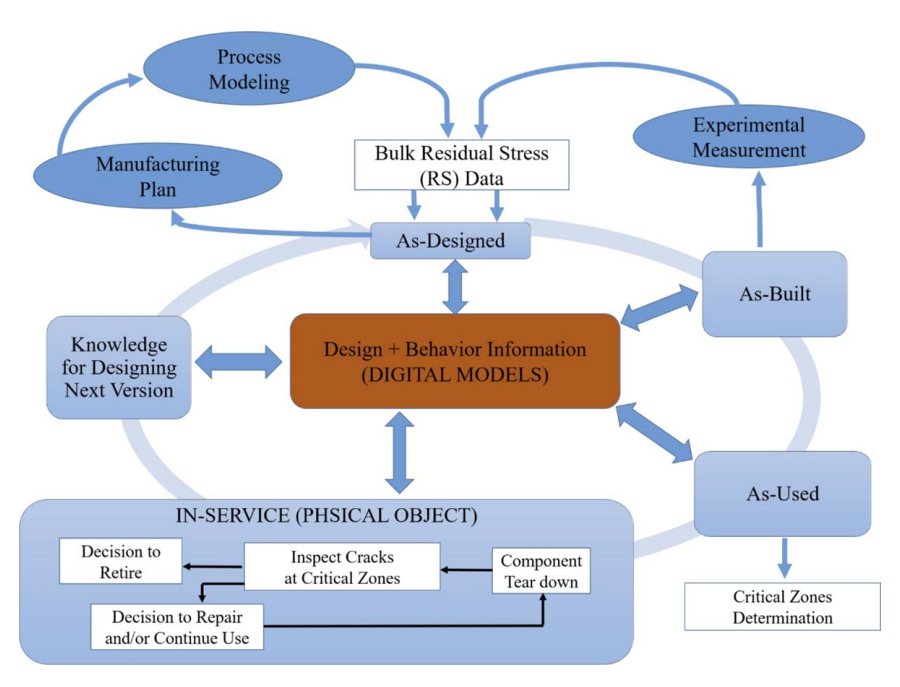


Fig. 11 Diagram representing the flow of data across the product lifecycle using digital models

spatial coordinates of the geometric location ahead of the initial (assumed) crack were searched in each of the two zone locations, from the CAD model with predicted in-service stresses and the four CAD models containing residual stress fields, in which the radial stress component (σ_{rr}) values were located. In zone 1, the σ_{RS} values obtained from the four turbine disk models are $\sigma_{RS} = -113$ MPa, $\sigma_{RS} = -14$ MPa, $\sigma_{RS} = -136$ MPa, $\sigma_{RS} = -37$ MPa, respectively. Whereas, in zone 2, the σ_{RS} values obtained from the four turbine disk models are $\sigma_{RS} = 22$ MPa, $\sigma_{RS} = 57$ MPa, σ_{RS} = 46 MPa, σ_{RS} = -16 MPa, respectively. For the case of this simplified analysis, the residual stress field did not evolve or redistribute for the four CAD models, as the crack was propagating. Since the turbine disk CAD models each have the same nominal geometry, the coordinate systems are the same between the models. Hence, the metadata from a particular location has been extracted without any associated issues in mismatch between the coordinate systems. After obtaining all the required stress fields, Eq. (5) is used to calculate the predicted life for the crack to grow to a critical length in the presence of the predicted residual stress fields. The crack growth (a) versus number of cycles (N) for the two zones are as shown in Fig. 10.

As shown in Figs. 10(a) and 10(b), the variations in residual stresses from the process modeling efforts, analogous to part-to-part variations, have resulted in variability or scatter in the estimated life at the two zones of interest. The inclusion of predicted behavior definitions within the design definition, and its exchange using the CAD models for forecasting component performance, has been enabled by the developed tool. By doing so, the potential for a network of models that define the component design behavior under particular operating conditions exists, which would begin to form the as-designed digital twin of the turbine disk by closing the loop between design, manufacturing and use. After the disk components are retired from application, the collection of digital material behavior attributes embedded in the CAD models contribute as a source of knowledge for design, repair, or re-design activities. By comparing the performance of the as-built disks, the variations can be evaluated for two purposes: (1) to inform the decision-making during design and manufacturing of the newer disk component and (2) to update and improve the accuracy of existing predictive models used in the digital twin framework. By analyzing a representative sample of disks according to similar techniques, after they have been removed from use at end of life (as-used), additional behavioral and contextual data can be gathered to increase the accuracy and validity of the product's model-based definition.

The use case presented in this paper demonstrated the capability of the developed tool to integrate behavior definitions into CAD models during the design stage in order to enable the as-designed digital twin. However, this capability of integrating models and exchanging stored lifecycle definitions (as shown in Fig. 11), from one model to another, can be incorporated to form the as-built digital twins or virtual replica of a produced component [37]. During the manufacturing of turbine disk components, geometric variations are inevitable, originating from the manufacturing process variability. The geometric variations in the manufactured disks can be directly measured and modeled by creating varying geometric instances of the CAD models, representing serialized part numbers for each disk of the as-built geometry and the modelbased definition of the residual stress distributions (given the geometric variation). By being able to associate material characterizations to geometric definitions in specific places on the topology of the model, the ability to track that connection through the lifecycle becomes easier and less prone to error.

Using the procedure to evaluate the location-specific, damage-tolerant fatigue life, in-service inspection schedules can be formulated uniquely for each manufactured disk—governed by their underlying residual stress distributions. For example, inspection and maintenance intervals are typically planned and performed at 50% of the remaining predicted life [38]. Based on the knowledge of the as-built geometry and corresponding model-based definition of residual stress for this geometry, a reasonable interval for

inspection and maintenance can be identified with a reduced level of uncertainty for each serialized disk (Fig. 11). As shown in the present use case, the embedding tool can enable this propagation of process models (in this case residual stress analysis) to downstream performance analysis (e.g., damage tolerance analysis of the fatigue lifetime). Hence, the CAD model serves to integrate disparate information sets throughout the produce lifecycle and provides a more robust information artifact than a CAD model that references a paper-based specification through a company's product data management or enterprise resource planning systems [39].

5 Conclusion

This paper presented a framework that expands the capability and capacity of a model-based definition (MBD) to capture spatially varying behavioral definitions in a complex object. By creating this capability as a plug-in for the CAD software, the user can store and retrieve metadata from spatial locations within the CAD model, which allows the CAD model to serve as a vehicle to integrate model-based data across the complete lifecycle. While the current example of the framework has been illustrated to capture manufacturing-induced bulk residual stress distributions using process modeling and characterization techniques within the design of a turbine disk component, this technique can be applied to any component for which material behavior information is known. However, with current CAD software technology, one must use the CAD software's SDK to access command-level functionality in order to establish the structure for each parameter type. The uncertainties in the predicted residual stress fields, also analogous to part-to-part variation, are used to create four instances of the CAD model to propagate downstream in life prediction analysis. The key findings from this work are as follows:

- (1) The work demonstrates the inclusion and exchange of lifecycle data to be stored within the CAD model of a part, which can reduce the likelihood of error caused by more direct human interaction with the data. Less human interaction by manipulating data values can also enhance the quality of information (by including spatially varying behavior). This framework creates new opportunities to utilize component behavioral information to explore additional parameters for performance-based design, potentially reducing the number of iterations during the design and production planning process.
- (2) A specific use case has been demonstrated using residual stress data, predicted via process modeling and experimentally characterized, and stored spatially within the CAD model of a turbine disk. Part-to-part variations have been captured based on the uncertainty in the residual stress models and propagated to identify the subsequent variability in the predicted fatigue life, via a damage tolerance analysis, at specific locations within the turbine disk. Historically, this type of information would have been captured in textual form, often paper-based, with no direct ability to connect it consistently to the geometry to which it was related. By being able to capture this information digitally within the model, the designer (and others) is able to maintain the connectivity and provenance of information.
- (3) The tool uses point objects as containers for storing behavior information, which act as spatial attribute markers indexed by its location coordinates. These indexed attribute markers in the MBD-CAD models allow integration of data from disparate models. Moreover, using the most basic form of geometric entity within the CAD system reduces the potential for data translation errors while exporting from the original CAD software tool. This ability to interconnect model definitions, enabled by the tool, is necessary to create a digital twin framework where the datasets from the models can be used for: (a) informing decision-making during design, manufacturing, and sustainment activities of the

- next version of the component and (b) update and reduce the uncertainty of existing predictive models used in the digital twin framework.
- (4) Creating a more robust, information-rich digital artifact cannot be overstated. Historically, technical drawings, reports, and specification documents had incredibly rich information in them regarding component geometry and material characteristics (among other information), and CAD tools only held geometry and geometry-related metadata. The technique illuminated in this paper will more readily enable industry's transition to the use of model-based definitions by making the CAD model artifact as rich in information as drawings and other paper-based documentation.

Acknowledgment

The authors would like to thank Alex Miller and Ramon Alvarez for their work in developing the CAD-based plug-in tool. Also, the authors appreciate the residual stress dataset produced by the consortium partners of the MAI-FEP bulk residual stress program, under principal investigator, Dr. Vasisht Venkatesh (Pratt & Whitney) and program manager, Dr. T.J. Turner (Air Force Research Laboratory).

Funding Data

 MDS would like to acknowledge funding from the National Science Foundation under CMMI 16-51956, and the IN-MaC faculty fellow program, which supported this work.

Conflict of Interest

There are no conflicts of interest.

Data Availability Statement

The datasets generated and supporting the findings of this article are obtainable from the corresponding author upon reasonable request.

Nomenclature

 $a = \operatorname{crack} \operatorname{length}$

m = Walker exponent

n = Paris' law exponent

w = width of the section through which the crack propagates

C = Paris' law coefficient

R =fatigue stress ratio

 a_i = initial crack length

 a_f = final crack length

 K_{max} = stress intensity factor for maximum load

 N_f = number of fatigue life cycles for crack to grow from

da initial to final crack length

 $\frac{dd}{dN}$ = fatigue crack growth rate

 $F\left(\frac{a}{w}\right)$ = geometric correction factor

MAI-FEP = Metals Affordability Initiative—Foundational

Engineering Problem

SDK = Software Development Kit

2D = Two dimensional

3D = Three dimensional

 ΔK_{eff} = effective stress intensity range

 $\sigma_{I,min}$ = maximum principal stress corresponding to minimum

service load

 $\sigma_{I,max}$ = maximum principal stress corresponding to

maximum service load

 σ_{RS} = residual stress component in the direction of applied maximum principal stress

Appendix: Determination of Geometric Correction Factor Expression, F(a/w)

A finite element approach is used to determine the geometric correction factors that apply for cracks at locations 1 and 2 (shown in Fig. 9(b) of the disk. The process involves simulating the nominal stresses without the presence of a crack in the model and simulating the stress response with explicitly insertion of cracks at these model locations. Simulations have been repeated with cracks of increasing lengths at each zone location to obtain the stress fields ahead of the crack in each simulation. The ratio of the maximum stress field ahead of the crack tip versus the stress present in the simulations without a crack (Sec. 4.2) forms the dataset for obtaining the geometric correction factor as a function of crack length for each location. A blunt tip crack with the shape of a U notch has been explicitly modeled in each location, with the initial crack length (a_i) of length a = 0.10 mm and constant width (w = 0.5 mm). Material properties applied to the crack section were E=10 Pa (several magnitudes lower than the material property in disk section), $\nu =$ 0.3 and a density $\rho = 0.599 \text{ kg/m}^3$ (density of air at 600 °C). Linear, quadrilateral mesh elements have been used for the analysis. The mesh has been refined around the crack geometry and a mesh sensitivity analysis was performed to identify the appropriate resolution ahead of the crack tip. The simulations have been performed using the same loads and boundary conditions as described in Sec. 4.2 for six different increasing crack sizes in each zone to obtain the maximum principal stresses ahead of the crack tip. For each zone, the datasets are fit using a second-order and third-order polynomials to obtain the $F(a/w)_{zone\ 1}$ and $F(a/w)_{zone\ 2}$, respectively, as shown

$$F\left(\frac{a}{w}\right)_{cone} = -107.9\left(\frac{a}{w}\right)^2 + 37.9\left(\frac{a}{w}\right) + 1 \tag{6}$$

$$F\left(\frac{a}{w}\right)_{zone} = 134.2\left(\frac{a}{w}\right)^3 - 77.24\left(\frac{a}{w}\right)^2 + 25.33\left(\frac{a}{w}\right) + 1$$
 (7)

References

- Gonzalez, C.,2016, "MachineDesign: What's the Difference Between Turbine Engines," https://www.machinedesign.com/motors-drives/article/21832035/whatsthe-difference-between-turbine-engines, Accessed 15 June, 2018.
- [2] Quintana, V., Rivest, L., Pellerin, R., Venne, F., and Kheddouci, F., 2010, "Will Model-Based Definition Replace Engineering Drawings Throughout the Product Lifecycle? A Global Perspective From Aerospace Industry," Comput. Ind., 61(5), pp. 497–508.
- [3] Sangid, M. D., and Matlik, J. F., 2016, "ANALYSIS A Better Way to Engineer Aerospace Components," Aerospace America, 54(3), pp. 40–43.
- [4] Qian, L., and Gero, J. S., 2010, "Function–Behavior–Structure Paths and Their Role in Analogy-Based Design," Artif. Intell. Eng. Des. Anal. Manuf., 10(4),
- [5] Ruemler, S. P., Zimmerman, K. E., Hartman, N. W., Hedberg, T., and Barnard Feeny, A., 2016, "Promoting Model-Based Definition to Establish a Complete Product Definition," ASME J. Manuf. Sci. Eng., 139(5), p. 051008.
- [6] Hedberg, T., Lubell, J., Fischer, L., Maggiano, L., and Barnard Feeney, A., 2016, "Testing the Digital Thread in Support of Model-Based Manufacturing and Inspection," ASME J. Comput. Inf. Sci. Eng., 16(2), p. 021001.
 [7] Camba, J., and Contero, M., 2015, "Assessing the Impact of Geometric Design
- [7] Camba, J., and Contero, M., 2015, "Assessing the Impact of Geometric Design Intent Annotations on Parametric Model Alteration Activities. Computers in Industry. 71:35–45. Copyright Elsevier," Comput. Ind., 71, pp. 35–45.
- [8] Feeney, A. B., Frechette, S. P., and Srinivasan, V., 2014, "A Portrait of an ISO STEP Tolerancing Standard as an Enabler of Smart Manufacturing Systems," ASME J. Comput. Inf. Sci. Eng., 15(2), p. 021005.
- [9] Furrer, D. U., Dimiduk, D. M., Cotton, J. D., and Ward, C. H., 2017, "Making the Case for a Model-Based Definition of Engineering Materials," Integr. Mater. Manuf. Innov., 6(3), pp. 249–263.
- [10] Miller, A. M., Hartman, N. W., Feeney, A. B., and Zahner, J., 2017, "Towards Identifying the Elements of a Minimum Information Model for Use in Model-Based Definition," International Manufacturing Science and Engineering Conference, Los Angeles, CA, June 4–8, Vol. 50749, p. V003T04A017.
- [11] Hedberg, T., Feeney, A. B., Helu, M., and Camelio, J. A., 2017, "Toward a Lifecycle Information Framework and Technology in Manufacturing," ASME J. Comput. Inf. Sci. Eng., 17(2), pp. 1–13.
- [12] Hedberg, T. D., Bajaj, M., and Camelio, J. A., 2020, "Using Graphs to Link Data Across the Product Lifecycle for Enabling Smart Manufacturing Digital Threads," ASME J. Comput. Inf. Sci. Eng., 20(1), pp. 1–15.

- [13] Schleich, B., Anwer, N., Mathieu, L., and Wartzack, S., 2017, "Shaping the Digital Twin for Design and Production Engineering," CIRP Ann.—Manuf. Technol., 66(1), pp. 141–144.
- [14] Grieves, M., and Vickers, J., 2017, "Digital Twin: Mitigating Unpredictable, Undesirable Emergent Behavior in Complex Systems," *Transdisciplinary Perspectives on Complex Systems*, F.-J. Kahlen, S. Flumerfelt, and A. Alves, eds., Springer, Cham, Switzerland, pp. 85–113.
- [15] Webster, G. A., and Ezeilo, A. N., 2001, "Residual Stress Distributions and Their Influence on Fatigue Lifetimes," Int. J. Fatigue, 23(Supplement 1), pp. 375–383.
- [16] Withers, P. J., and Bhadeshia, H. K. D. H., 2001, "Residual Stress. Part 2—Nature and Origins," Mater. Sci. Technol., 17(4), pp. 366–375.
- [17] Rolph, J., Preuss, M., Iqbal, N., Hofmann, M., Nikov, S., Hardy, M. C., Glavicic, M. G., Ramanathan, R., and Evans, A., 2012, "Residual Stress Evolution During Manufacture of Aerospace Forgings," Superalloys 2012: 12th International Symposium on Superalloys. pp. 881–891.
- [18] Gayda, J., 2001, "The Effect of Heat Treatment on Residual Stress and Machining Distortions in Advanced Nickel Base Disk Alloys," NASA/ TM-2001-210717, Jan.
- [19] Ma, K., Goetz, R., and Svrivatsa, S. K., 2010, "Modeling of Residual Stress and Machining Distortion in Aerospace Components," ASM Handbook. Vol. 22B: Metals Process Simulation.
- [20] Fluhrer, J., 2006, "DEFORM 3D User's Manual Version 6. 0", Scientific Forming Technologies Corporation, Columbus, OH.
- [21] Nelson, D., 1982, "Effects of Residual Stress on Fatigue Crack Propagation," Residual Stress Effects in Fatigue, J. Throop and H. Reemsnyder, eds., ASTM, West Conshohocken, PA, pp. 172–194.
- [22] Lammi, C. J., and Lados, D. A., 2012, "Effects of Processing Residual Stresses on Fatigue Crack Growth Behavior of Structural Materials: Experimental Approaches and Microstructural Mechanisms," Metall. Mater. Trans. A, 43(1), pp. 87–107.
- [23] John, R., Larsen, J. M., Buchanan, D. J., and Ashbaugh, N. E., 2001, "Incorporating Residual Stresses in Life Prediction of Turbine Engine Disks," Proceedings from NATO RTO (AVT) Symposium on Monitoring and Management of Gas Turbine Fleets for Extended Life and Reduced Costs, Manchester, UK, Oct. 8–11.
- [24] McClung, R., Enright, M., Liang, W., Chan, K., Moody, J., Wu, W.-T., Shankar, R., Luo, W., Oh, J., and Fitch, S., 2012, "Integration of Manufacturing Process Simulation With Probabilistic Damage Tolerance Analysis of Aircraft Engine Components," 53rd AIAA/ASME/ASCE/AHS/ASC Structures, Structural Dynamics and Materials Conference, Honolulu, HI, Apr. 23–26, pp. 1–13.
- [25] Cernatescu, I., Venkatesh, V., Glanovsky, J. L., Landry, L. H., Green, R. N., Street, M., and Hartford, E., 2015, "Residual Stress Measurements Implementation for Model Validation as Part of Foundational Engineering Problem Program on ICME of Bulk Residual Stress in Ni Rotors," AIAA SciTech Conference Proceedings, 56th AIAA/ASCE/AHS/ASC Structures, Structural Dynamics, and Materials Conference, Kissimmee, FL, Jan. 5–9, pp. 1–9.
- [26] Withers, P. J., and Bhadeshia, H. K. D. H., 2001, "Residual Stress. Part 1– Measurement Techniques," Mater. Sci. Technol., 17(4), pp. 355–365.

- [27] Venkatesh, V., Green, R., O'Connell, J., Cernatescu, I., Goetz, R., Wong, T., Streich, B., Saraf, V., Glavicic, M., Slavik, D., Sampath, R., Sharp, A., Song, B., and Bocchini, P., 2018, "An ICME Framework for Incorporating Bulk Residual Stresses in Rotor Component Design," Integr. Mater. Manuf. Innov., 7(4), pp. 173–185.
- [28] Miller, A. M. D., Alvarez, R., and Hartman, N., 2018, "Towards an Extended Model-Based Definition for the Digital Twin," Comput. Aided Des. Appl., 15(6), pp. 880–891.
- [29] Cowles, B. A., Backman, D. G., and Dutton, R. E., 2015, "Update to Recommended Best Practice for Verification and Validation of ICME Methods and Models for Aerospace Applications," Integr. Mater. Manuf. Innov., 4(1), pp. 16–20.
- [30] Cláudio, R. A., Branco, C. M., Gomes, E. C., and Byrne, J., 2004, "Fatigue Life Prediction and Failure Analysis of a Gas Turbine Disc using the Finite-Element Method," Fatig. Fract. Eng. Mater. Struc., 27(9), pp. 849–860.
- [31] Cook, C. H., Spaeth, C. E., Hunter, D. T., and Hill, R. J., 1982, "Damage Tolerant Design of Turbine Engine Disks," ASME 82-GT-311, Am. Soc. Mech. Eng., New York.
- [32] Irwin, G. R., 1957, "Analysis of Stresses and Strains Near the End of a Crack Traversing a Plate," ASME J. Appl. Mech.-Trans. ASME, 24(Vol. E24), pp. 351–369.
- [33] Sangid, M. D., Stori, J. A., and Ferriera, P. M., 2010, "Process Characterization of Vibrostrengthening and Application to Fatigue Enhancement of Aluminum Aerospace Components—Part II: Process Visualization and Modeling," Int. J. Adv. Manuf. Technol., 53(5–8), pp. 561–575.
- [34] James, L. A., and Mills, W. J., 1985, "Effect of Heat-Treatment and Heat-to-Heat Variations in the Fatigue-Crack Growth Response of Alloy 718," Eng. Frac. Mech., 22(5), pp. 797–817.
- [35] Walker, K., 1970, "The Effect of Stress Ratio During Crack Propagation and Fatigue for 2024-T3 and 7075-T6 Aluminum," Effects of Environment and Complex Load History on Fatigue Life, M. Rosenfeld, ed., ASTM International, West Conshohocken, PA, pp. 1–14.
- [36] James, L. A., 1989, "Fatigue Crack Propagation in Alloy 718: A Review," Superalloy 718–Metallurgy and Applications, E. A. Loria, ed., The Minerals, Metals & Materials Society, Warrendale, PA, pp. 499–515.
- [37] Glaessgen, E., and Stargel, D., 2012, "The Digital Twin Paradigm for Future NASA and U.S. Air Force Vehicles," 53rd AIAA/ASME/ASCE/AHS/ASC Structures, Structural Dynamics and Materials Conference, Honolulu, HI, Apr. 23–26, pp. 1–14.
- [38] Annis, C. G., Cargill, J. S., Harris, J. A., and Van Wanderham, M. C., 1981, "Engine Component Retirement-for-Cause: A Nondestructive Evaluation (NDE) and Fracture Mechanics-Based Maintenance Concept," JOM J. Miner. Met. Mater. Soc., 33(7), pp. 24–28.
- [39] Lee, C., Leem, C. S., and Hwang, I., 2011, "PDM and ERP Integration Methodology Using Digital Manufacturing to Support Global Manufacturing," Int. J. Adv. Manuf. Technol., 53(1–4), pp. 399–409.